

A STUDY OF SMART FOAM FOR NOISE CONTROL APPLICATIONS

Cassandra A. Gentry-Grace

Dissertation Submitted to the Faculty of the
Virginia Polytechnic Institute & State University
in partial fulfillment of the requirements for the degree of
Doctor of Philosophy
in
Mechanical Engineering

Christopher R. Fuller, Chair

Ricardo A. Burdisso

Daniel J. Inman

Marty E. Johnson

Gary S. Robinson

October 28, 1998

Blacksburg, Virginia

Keywords: Smart foam, Active noise control, Passive noise control, Piezoelectric
actuator, Active structural acoustic control

Copyright 1998, Cassandra A. Gentry-Grace

A STUDY OF SMART FOAM FOR NOISE CONTROL APPLICATIONS

Cassandra A. Gentry-Grace

(ABSTRACT)

Smart foam is a composite noise control treatment that consists of a distributed piezoelectric actuator, known as polyvinylidene fluoride (PVDF), embedded within a layer of partially-reticulated polyurethane foam. The principal function of smart foam is to yield broadband sound attenuation. Passive acoustic foams are a very reliable high-frequency sound reduction method. With regard to smart foam, the embedded piezoelectric actuator is introduced to overcome the limitations of the passive foam in the low-frequency region. The piezoelectric actuator excites the structural and acoustic phases of the foam when driven by an externally supplied control voltage. This generates a secondary acoustic field which destructively interacts with the acoustic field created by a primary noise source. Initial experiments employ the composite “active/passive” treatment to yield attenuation of piston sound radiation. For this simple source, the global farfield pressure is minimized according to the feedforward, Filtered-x LMS control algorithm using one error sensor. Significant broadband sound attenuation is obtained. A more advanced noise control problem is investigated which minimizes plate radiation. The vibrating plate has a distributed modal response requiring a collective array of independently-phased smart foam actuators to yield reduction of the radiated sound power. This is accomplished by minimizing the sound pressure at an array of nearfield microphones. Good broadband sound power reduction is obtained using a MIMO (multiple-input/multiple-output) Filtered-x LMS control scheme. Various techniques for improving smart foam’s acoustic control authority are identified during manufacturing and finite element modeling. of the actuator. These improved smart foam actuators are employed as an active/passive liner to suppress the transverse propagating acoustic modes within an anechoically-terminated rectangular duct. A section of a duct wall is lined with an array of smart foam and the sound downstream of the control actuators is minimized at

several error microphones. Successful harmonic and broadband noise control is achieved. A full-scale numerical model of the duct acoustic control application is presented based on the finite element method. The purpose of the model is to study the sensitivity of this active/passive control approach relative to the spatial distribution of control channels and error sensors. A comparison of the numerical and experimental results yields similar trends.

ACKNOWLEDGEMENTS

I extend my sincerest appreciation to Dr. Chris Fuller who served as the academic advisor for this research. During the completion of this work, his expert knowledge of structural acoustics and active noise control proved to be invaluable. I thank him for the opportunity to do interesting, challenging and independent research and for his support as a mentor. I am grateful to Dr. Ricardo Burdisso, committee member and professor in the areas of structural vibration and acoustics. As a student who entered the program with little prior knowledge of acoustics, the clarity of his lectures and his willingness to confer with students on a regular basis was greatly appreciated. I thank Dr. Dan Inman, Dr. Marty Johnson and Dr. Gary Robinson for serving on this committee. I appreciate all of the committee members taking the time to review this dissertation and for providing helpful suggestions and critiques.

A special acknowledgment is owed to Dr. Cathy Guigou, former committee member and friend, in recognition of her enthusiastic guidance and helpful technical discussions during much of this research. I express appreciation to all of the VAL staff and student's who have helped me in many ways. I acknowledge Dr. David Swanson, who served as my academic advisor during my graduate studies at Penn State. With his mentoring, I decided to pursue a Ph.D. with an emphasis in acoustics. On several occasions during my tenure at Virginia Tech, he communicated words of encouragement and advice which were greatly appreciated.

I am grateful to NASA LaRC for granting me the financial support to complete this research through the GSRP (Graduate Student Researcher's Program). I acknowledge Dr. Joe Posey for serving as the NASA representative on this project and for giving me opportunities to present my work at the LaRC facility.

Many who have pursued a Ph.D. know that it can be a lengthy process with times of triumphs and adversities. There are many friends and relatives who have contributed their support to make this achievement possible. Unfortunately, I cannot acknowledge everyone but there are three people who I must take this opportunity to thank. To my dear parents, Dr. and Mrs. Theartice Gentry, words cannot express how grateful I am to you as I approach the end of my academic career. Your unwavering love, strength and support

for my personal and academic endeavors has always been a true source of inspiration. Don't ever forget that you can always count on me. A very special expression of thanks is owed to my loving husband, Dr. Christopher Grace, whose devotion and sense of humor is always uplifting. You stood by me at every step of the way. I am very proud and blessed to have you as my partner in life.

TABLE OF CONTENTS

ABSTRACT	ii
ACKNOWLEDGEMENTS	iv
LIST OF FIGURES	ix
LIST OF TABLES	xvi
i	
CHAPTER 1: <u>Introduction to Active/Passive Structural Acoustic Control</u>	
1.1 Motivation of study	1
1.2 Recent Literature on Active Surface Treatments	5
1.3 Organization of thesis.....	10
CHAPTER 2: <u>The Manufacturing of Smart Foam and a Simple Source Noise Control Application</u>	
2.1 Introduction	13
2.2 Smart Foam Components	15
2.3 Smart Foam Construction.....	18
2.4 Piston Radiation Control Experimental Setup & Procedure	22
2.5 Comparison of Acoustic Behavior of Various Actuator Configurations	24
2.6 Passive Effect of Smart Foam on Sound Radiation	27
2.7 Harmonic Radiation Control Results	28
2.8 Broadband Radiation Control Results.....	31
2.9 Feasibility of Implementing a Nearfield Error Microphone.....	34
2.10 A Note about Smart Foam Bonding Layer and Lead Attachment.....	35
2.11 Summary	37
CHAPTER 3: <u>Plate Radiation Control with Smart Foam</u>	
3.1 Introduction	38
3.2 Experimental Setup	39
3.2.1 The Noise Source	39
3.2.2 The Control Actuators	41
3.2.3 The Error Sensors.....	43

3.3 Acoustic Power Measurement Technique.....	44
3.4 Experimental Procedure.....	45
3.5 Experimental Results.....	45
3.5.1 Harmonic Control Results.....	45
3.5.2 Broadband control 1110 case with a single smart foam module.....	47
3.5.3 Broadband control 1110 case with multiple smart foam modules operating in phase.....	49
3.5.4 Broadband control 6160 case with multiple, independent smart foam modules.....	51
3.6 Summary.....	55
CHAPTER 4: <u>Numerical Modeling of Smart Foam</u>	
4.1 Introduction.....	57
4.2 Overview of Poroelastic Material Theory Development.....	60
4.3 Biot Theory of Sound Propagation in Isotropic, Elastic Porous Materials.....	63
4.3.1 Stress-Strain Relations.....	64
4.3.2 Kinetic Energy Density.....	68
4.3.3 Dissipation Function.....	68
4.3.4 Equations of Motion for an Isotropic, Elastic Porous Material.....	69
4.4 The Compressional Waves.....	70
4.5 The Shear Wave.....	72
4.6 The Three Biot Waves in Air-Saturated Acoustic Foam.....	73
4.7 Example Application: Prediction of Surface Impedance at Normal Incidence for a Layer of Porous Material Backed by a Rigid Wall.....	77
4.8 The Finite Element Method.....	82
4.9 Finite Element Formulation for Poroelastic Media.....	84
4.9.1 Verification of Poroelastic Finite Element Model.....	87
4.10 Finite Element Formulation for Ideal Fluids.....	91
4.10.1 Verification of Acoustic Finite Element Model.....	92
4.11 Finite Element Formulation of Piezoelectric Actuator.....	95
4.12 Coupling of Poroelastic Finite Elements with Acoustic Finite Element.....	102

4.12.1 Verification of Coupling of Poroelastic and Acoustic Finite Elements	104
4.13 Coupling of the Poroelastic and Piezoelectric Finite Elements	106
4.14 Smart Foam Simulation by the Finite Element Method.....	106
4.15 Summary	111
CHAPTER 5: <u>Smart Foam as an Active/Passive Liner for Duct Acoustic Control:</u>	
<u>Experimental and Numerical Studies</u>	
5.1 Introduction	113
5.2 Duct Properties and Construction	114
5.3 Modal Analysis of Interior Acoustic Field of Duct & Reflection Coefficient Describing Duct Termination.....	116
5.4 Smart Foam Module Properties and Construction	124
5.5 Duct Acoustic Control Experimental Setup & Procedure.....	126
5.6 Experimental Results	130
5.6.1 Acoustic Characteristics of Smart Foam Actuators	130
5.6.2 Harmonic Control: 2I2O & 3I3O Cases @ 184 Hz.....	133
5.6.3 Harmonic Control: 2I2O & 3I3O Cases @ 342 Hz.....	139
5.6.4 Harmonic Control: 3I3O & 4I3O Cases @ 504 Hz.....	145
5.6.5 Broadband Control: 4I3O Case @ $100 < f < 525$ Hz.....	149
5.7 Comparison of Numerical and Experimental Duct Noise Control Results.....	154
5.8 Summary	168
CHAPTER 6: <u>Concluding Discussion</u>	
6.1 Key Accomplishments	169
6.2 Future Work	174
References	176
APPENDIX A: Plots of Raw Data for Duct Noise Control Experiment	183
Vita.....	184

LIST OF FIGURES





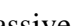







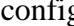
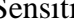
Figure 2.1: Illustration of smart foam active/passive noise control actuator.	14
Figure 2.2: Piezo film dipole alignment.....	16
Figure 2.3: Numerical classification of piezo film axes.....	17
Figure 2.4: Piezo film displacement motion under excitation.	19
Figure 2.5: PVDF actuator configurations, (a) Original, (b) Parallel and (c) Series-Parallel.	21
Figure 2.6: Piston radiation control experimental setup.	23
Figure 2.7: Smart foam behavior at 290 Hz for different PVDF actuator configurations (silicone adhesive used); (a) SPL under 100 V rms. input voltage, (b) Sensitivity and (c) Harmonic Distortion.....	26
Figure 2.8: Passive effects of embedded PVDF layer on global sound level;  Piston,  Plain foam,  Smart foam	28
Figure 2.9: Harmonic control results at (a) 290 Hz and (b) 1000 Hz;  Piston,  Passive,  Active/Passive series-parallel configuration,  Active/Passive parallel configuration.	30
Figure 2.10: Broadband control results; (a) SPL at error microphone; (b) global sound level;  Piston,  Passive,  Active/Passive series-parallel configuration,  Active/Passive parallel configuration.	33
Figure 2.11: Comparison of global sound attenuation offered by nearfield and farfield error sensors;  Passive,  Active/Passive (farfield control),  Active/Passive (nearfield control).	35
Figure 2.12: Smart foam behavior at 290 Hz for different PVDF actuator configurations (spray glue adhesive used); (a) SPL under 100 V rms. input voltage, (b) Sensitivity and (c) Harmonic Distortion.	36
Figure 3.1 (a) Illustration of front of plate. (b) Illustration of rear of plate.....	40
Figure 3.2: (a) Smart foam module. (b) Power radiated by a single smart foam	42
Figure 3.3: Distributed smart foam actuators and error sensor configuration.....	43
Figure 3.4: Spherical dome for power measurements.	44

Figure 3.5: (a) Active/passive SPL reduction of (3,1) plate mode at 545 Hz.	
(b) Active/passive power reduction of (3,1) plate mode at 545 Hz.	46
Figure 3.6. Experimental setup for IIO broadband control case.....	47
Figure 3.7: Radiated power for broadband IIO control case using a single smart foam module.....	49
Figure 3.8: Radiated power for broadband IIO control case using multiple smart foam modules operating in phase.	50
Figure 3.9: Average attenuated SPL at the error microphone array for broadband 6I6O control case using multiple, independent smart foam modules.....	52
Figure 3.10: Attenuated power for broadband 6I6O case using multiple-independent smart foam modules	53
Figure 3.11: Radiated power for broadband 6I6O control case using multiple, independent smart foam modules.	54
Figure 4.1 Illustration of a generic porous material and the macroscopic modeling approach.....	58
Figure 4.2 State of stress in the solid and fluid phases of an elementary macroscopic volume of porous material.....	64
Figure 4.3(a): Variation of the normalized phase speed of the P1, P2 and S waves propagating in acoustic foam with respect to frequency.....	76
Figure 4.3(b): Variation of the attenuation coefficient of the P1, P2 and S waves propagating in acoustic foam with respect to frequency.....	77
Figure 4.4 Illustration of a porous layer bonded to a rigid foundation and excited by a normal incident plane acoustic wave.....	78
Figure 4.4 Illustration of a porous layer bonded to a rigid foundation and excited by a normal incident plane acoustic wave.....	81
Figure 4.5(a): Normalized surface impedance vs. frequency of Glass wool. The thickness of the layer is 5.6 cm. Normalized impedance of glass wool: ————. Normalized impedance of similar rigid framed material: - - - - -	83

Figure 4.5(b): Normalized surface impedance vs. frequency of acoustic foam. The thickness of the layer is 2.0 cm. Normalized impedance of acoustic foam: ————. Normalized impedance of similar rigid framed material: - - - - - 83

Figure 4.6. Illustration of *discretized* finite element model of smart foam in an air-filled duct. 83

Figure 4.7: Illustration of a problem solved using numerical poroelastic model and sample finite element mesh of the system. 88

Figure 4.8: Surface displacement of Glass Wool due to mechanical force. A comparison of analytical and FEM results. 89

Figure 4.9: Surface displacement of partially-reticulated foam due to mechanical force. A comparison of analytical and FEM results 90

Figure 4.10: Illustration of a problem solved using numerical acoustic model and sample finite element mesh of the system. 93

Figure 4.11: Verification of FEM model of acoustic system. Average SPL at $x=0$ and $x=L$ vs. frequency for rigid air-filled duct excited by an oscillating piston. 94

Figure 4.12: Verification of FEM model of acoustic system. Average SPL at $x=0$ and $x=L$ vs. frequency for rigid air-filled duct with anechoic termination excited by an oscillating piston. 95

Figure 4.13(a): Piezoelectric finite element with one degree of freedom per node (b) Piezoelectric finite element with two degrees of freedom per node (c) Assembly of piezoelectric finite elements to establish cylindrical actuator of radius, R 96

Figure 4.14(a): Horizontal displacement of PVDF actuator with “free” boundary conditions at 250 Hz with 300 V rms excitation. (b) Vertical displacement of PVDF actuator with “free” boundary conditions at 250 Hz with 300 V rms excitation. 99

Figure 4.15(a): Horizontal displacement of PVDF actuator with “fixed” boundary conditions at 250 Hz with 300 V rms excitation. (b) Vertical displacement of PVDF actuator with “fixed” boundary conditions at 250 Hz with 300 V rms excitation. 100

Figure 4.16: Average vertical displacement of PVDF actuator with “fixed” boundary conditions vs. frequency with 300 V rms excitation. 101

Figure 4.17: Illustration of acoustic waveguide terminated by a foam layer. Represents system used verify finite element acoustic-poroelastic coupling procedure.	104
Figure 4.18: Comparison of normalized acoustic impedance as determined by analytical and finite element methods (a) Real part. (b) Imaginary part.....	105
Figure 4.19: Comparison of normal incidence absorption coefficient as determined by analytical and finite element methods.	106
Figure 4.20 Illustration of smart foam actuator configurations investigated using the finite element approach. Smart foam with embedded PVDF shaped as (1) Four free triangles, (2) Four free half-cylinders (3) Eight free triangles, (4) Eight free half-cylinders, (5) Four fixed triangles, (6) Four fixed half-cylinders, (7) Eight fixed triangles, and (8) Eight fixed half-cylinders.....	109
Figure 4.21: Sound pressure level vs. frequency generated by various smart foam array configurations excited at $300 V_{rms}$ while positioned in rigid duct with anechoic termination (a) Smart foam with embedded PVDF shaped as half-cylinders (b) Smart foam with embedded PVDF shaped as triangles.....	110
Figure 5.1 Interior dimensions of duct.	114
Figure 5.2 (a) Duct in the laboratory. (b) Acoustic speaker in duct end wall. (c) Anechoic wedge at duct termination.	115
Figure 5.3 Illustration of one dimensional acoustic mode shapes within duct.....	116
Figure 5.4: The four unique duct configurations used for acoustic modal analysis (a) Rigid duct floor with anechoic termination (b) Rigid duct floor with rigid termination (c) Foam-lined duct floor with anechoic termination (d) Foam-lined duct floor with rigid termination	117
Figure 5.5: Comparison of acoustic energy vs. frequency for Rigid Duct/Rigid End and Rigid Duct/Anechoic End configurations.	121
Figure 5.6: Comparison of acoustic energy vs. frequency for Rigid Duct/Anechoic End and Lined Duct/Anechoic End configurations.	121
Figure 5.7 Comparison of acoustic energy vs. frequency for Lined Duct/Rigid End and Lined Duct/Anechoic End configurations	122

Figure 5.8: Comparison of acoustic energy vs. frequency for Rigid Duct/Rigid End and Lined Duct/Rigid End configurations	122
Figure 5.9: Power reflection coefficient vs. frequency for the anechoically-terminated, rigid duct.	124
Figure 5.10: (a) Top view of single smart foam module used in duct experiments (b) Bottom view of single smart foam module used in duct experiments.	126
Figure 5.11: Experimental setup for duct acoustic control experiment.	127
Figure 5.12 MIMO Feedforward filtered-x control algorithm.	129
Figure 5.13. (a) Array of observation microphones located in the cross section of the duct. (b) Array of smart foam actuators on the bottom wall of the duct	130
Figure 5.14: Smart foam acoustic response vs. voltage input (a) at harmonics of 184 Hz (b) at harmonics of 342 Hz (c) at harmonics of 504 Hz.....	132
Figure 5.15: 2I2O Harmonic Control at 184 Hz with error microphones 1,16 (a) <i>Upstream</i> SPL vs. Transverse duct position (b) <i>Downstream</i> SPL vs. Transverse duct position.....	136
Figure 5.16: 2I2O Harmonic Control at 184 Hz with error microphones 1,8 (a) <i>Upstream</i> SPL vs. Transverse duct position (b) <i>Downstream</i> SPL vs. Transverse duct position.....	137
Figure 5.17: 3I3O Harmonic Control at 184 Hz with error microphones 1,8,16 (a) <i>Upstream</i> SPL vs. Transverse duct position (b) <i>Downstream</i> SPL vs. Transverse duct position.....	138
Figure 5.18: 2I2O Harmonic Control at 342 Hz with error microphones 1,16 (a) <i>Upstream</i> SPL vs. Transverse duct position (b) <i>Downstream</i> SPL vs. Transverse duct position.....	142
Figure 5.19: 2I2O Harmonic Control at 342 Hz with error microphones 3,10 (a) <i>Upstream</i> SPL vs. Transverse duct position (b) <i>Downstream</i> SPL vs. Transverse duct position.....	143
Figure 5.20: 3I3O Harmonic Control at 342 Hz with error microphones 1,8,16 (a) <i>Upstream</i> SPL vs. Transverse duct position (b) <i>Downstream</i> SPL vs. Transverse duct position.....	144

Figure 5.21: 3I3O Harmonic Control at 504 Hz with error microphones 1,8,16 (a) <i>Upstream</i> SPL vs. Transverse duct position (b) <i>Downstream</i> SPL vs. Transverse duct position.....	147
Figure 5.22: 4I3O Harmonic Control at 504 Hz with error microphones 1,6,11,16 (a) <i>Upstream</i> SPL vs. Transverse duct position. (b) <i>Downstream</i> SPL vs. Transverse duct position.....	148
Figure 5.23: 4I3O Broadband Control $175 < f < 525$ with error microphones 1,6,11,16 (a) <i>Upstream</i> SPL vs. Frequency (b) <i>Downstream</i> SPL vs. Frequency.....	151
Figure 5.24: 4I3O Broadband Control at $175 < f < 525$ with error microphones 1,6,11,16 Average Control Voltage to Smart Foam Channel 1,2 and 3 vs. Frequency.	152
Figure 5.25: 4I3O Broadband Control $250 < f < 350$ Hz with error microphones 1,6,11,16 (a) <i>Upstream</i> SPL vs. Frequency (b) <i>Downstream</i> SPL vs. Frequency	153
Figure 5.26: 1I1O Harmonic Control @ 188 Hz (a) <i>Upstream</i> SPL vs Transverse Duct Position (b) <i>Downstream</i> SPL vs. Transverse Duct Position.....	160
Figure 5.27: 2I2O Harmonic Control @ 188 Hz (a) <i>Upstream</i> SPL vs. Transverse Duct Position (b) <i>Downstream</i> SPL vs. Transverse Duct Position.....	161
Figure 5.28: 1I1O Harmonic Control @ 349 Hz (a) <i>Upstream</i> SPL vs. Transverse Duct Position (b) <i>Downstream</i> SPL vs. Transverse Duct Position.....	162
Figure 5.29: 2I2O Harmonic Control @ 349 Hz (a) <i>Upstream</i> SPL vs. Transverse Duct Position (b) <i>Downstream</i> SPL vs. Transverse Duct Position.....	163
Figure 5.30: 3I3O Harmonic Control @ 349 Hz (a) <i>Upstream</i> SPL vs. Transverse Duct Position (b) <i>Downstream</i> SPL vs. Transverse Duct Position.....	164
Figure 5.31: 1I1O Harmonic Control @ 509 Hz (a) <i>Upstream</i> SPL vs. Transverse Duct Position (b) <i>Downstream</i> SPL vs. Transverse Duct Position.....	165
Figure 5.32: 2I2O Harmonic Control @ 509 Hz (a) <i>Upstream</i> SPL vs. Transverse Duct Position (b) <i>Downstream</i> SPL vs. Transverse Duct Position.....	166
Figure 5.33: 3I3O Harmonic Control @ 509 Hz (a) <i>Upstream</i> SPL vs. Transverse Duct Position (b) <i>Downstream</i> SPL vs. Transverse Duct Position.....	167
Figure A.1: 2I2O Harmonic Control at 184 Hz with error microphones 1,16 (a) <i>Upstream</i> SPL vs. Microphone Number (b) <i>Downstream</i> SPL vs. Microphone Number. Untreated Duct ———— , Passive Control ; Active/Passive Control	184

Figure A.2: 2I2O Harmonic Control at 184 Hz with error microphones 1,8 (a) *Upstream* SPL vs. Microphone Number (b) *Downstream* SPL vs. Microphone Number. Untreated Duct ———, Passive Control -----, Active/Passive Control 185

Figure A.3: 2I2O Harmonic Control at 184 Hz with error microphones 1,8,16 (a) *Upstream* SPL vs. Microphone Number (b) *Downstream* SPL vs. Microphone Number. Untreated Duct ———, Passive Control -----, Active/Passive Control 186

Figure A.4: 2I2O Harmonic Control at 342 Hz with error microphones 1,16 (a) *Upstream* SPL vs. Microphone Number (b) *Downstream* SPL vs. Microphone Number. Untreated Duct ———, Passive Control -----, Active/Passive Control 187

Figure A.5: 2I2O Harmonic Control at 342 Hz with error microphones 3,10 (a) *Upstream* SPL vs. Microphone Number (b) *Downstream* SPL vs. Microphone Number. Untreated Duct ———, Passive Control -----, Active/Passive Control 189

Figure A.6: 3I3O Harmonic Control at 342 Hz with error microphones 1,8,16 (a) *Upstream* SPL vs. Microphone Number (b) *Downstream* SPL vs. Microphone Number. Untreated Duct ———, Passive Control -----, Active/Passive Control 190

Figure A.7: 3I3O Harmonic Control at 504 Hz with error microphones 1,8,16 (a) *Upstream* SPL vs. Microphone Number (b) *Downstream* SPL vs. Microphone Number. Untreated Duct ———, Passive Control -----, Active/Passive Control 191

Figure A.8: 4I3O Harmonic Control at 504 Hz with error microphones 1,6,11,16 (a) *Upstream* SPL vs. Microphone Number (b) *Downstream* SPL vs. Microphone Number. Untreated Duct ———, Passive Control -----, Active/Passive Control 192

LIST OF TABLES

Table 3.1: Comparison of experimental resonant frequencies of bare plate and foam-covered plate.	40
Table 4.1: Important foam parameters and measurement techniques.	59
Table 4.2: Typical properties of glass wool.	74
Table 4.3: Typical properties of partially-reticulated acoustic foam.....	80
Table 5.1: Transverse & longitudinal acoustic duct resonance frequencies corresponding to the four unique duct configurations	120